Electrochimica Acta 409 (2022) 139971

Contents lists available at ScienceDirect

Electrochimica Acta

journal homepage: www.elsevier.com/locate/electacta

Understanding efficient phosphorus-functionalization of graphite for vanadium flow batteries

Hannes Radinger[a,*], Mark Hartmann[b], Marius Ast[a], Jessica Pfisterer[a], Michael Bron[b], Helmut Ehrenberg[a], Frieder Scheiba[a]

[a] Institute for Applied Materials, Karlsruhe Institute of Technology, Hermann-von-Helmholtz-Platz 1, D-76344 Eggenstein-Leopoldshafen, Germany
[b] Institute of Chemistry, Martin Luther University Halle-Wittenberg, Von-Danckelmann-Platz 4, D-06120 Halle (Saale), Germany

ARTICLE INFO

Article history:
Received 24 November 2021
Revised 21 January 2022
Accepted 24 January 2022
Available online 25 January 2022

Keywords:
Vanadium redox flow battery
Electrocatalytic activity
Graphite electrode
Phosphorus doping
Surface functionalization

ABSTRACT

Numerous surface treatment methods are known to enhance the electrochemical activity of graphite felt (GF), such as thermal activation or attachment of nanoparticulate catalysts. The integration of heteroatoms into the graphite lattice at the surface could be a promising technique for reliable and efficient electrode activation. However, these functionalization techniques are based on thermochemical activation, which makes it difficult to distinguish between activity effects other than foreign atom integration, such as defects and other surface groups that must be considered. In this work, we analyzed commercial and synthetic phosphorus-doped graphene and GF using different electrochemical and physicochemical techniques. Despite a high doping concentration, the activity of the commercial powder bonded to GF and coated on glassy carbon remained limited due to the low degree of graphitization and high oxygen content. Instead, a low phosphorus concentration of <1 at% combined with a high degree of graphitization increased the catalytic activity. Building on these findings, GF was rationally modified, resulting in twice the power density compared to the original material in full cell tests.

1. Introduction

As a key component of the vanadium flow battery (VFB), the graphite felt (GF) electrode determines the conversion efficiency of electrical to chemical energy and *vice versa*. Due to its slow charge transfer properties, lots of ongoing research and development focuses on improving the activity through appropriate pretreatments. In general, these processes can be divided into three subcategories: first, the activation of the electrode by thermal, chemical, or electrochemical treatments to alter the surface properties of GF, increase the surface area and introduce active sites[1–4]. Second, the decoration of GF by a variety of carbon-based materials such as graphene or carbon nanotubes, or metal-based material such as bismuth nanoparticles, TiC, or metal oxides[5–9]. Third, the direct integration of heteroatoms into the surface of graphite to increase the electron donor or acceptor levels which should enable more efficient charge transfer. Each tactic faces specific problems: surface functional groups and graphitic defects are often unstable during electrochemistry[10]. The binding of particles to GF is difficult because the flowing electrolyte can wash away the valuable catalyst material. Using a polymeric binder adds complexity to the process and may passivate parts of the electrode. In contrast, heteroatom functionalization might be able to reliably integrate active sites into the lattice of graphite, which do not depend on loose surface groups or can be easily removed by convective forces.

First-principle calculations already predicted the possibility to improve the catalytic activity of graphene for the negative vanadium half-cell reaction by heteroatom functionalization[11]. The effects of different nitrogen-containing groups were discussed and compared to graphitic boron and phosphorus groups. Regarding the electrical conductivity, wettability, and calculated energy barriers, phosphorus-modified graphene was the most promising approach. However, few experimental studies characterized an electrode treated with boron, phosphorus, nitrogen, or multiple elements for VFBs[12–16]. For boron-doped GF it was shown that not the amount of boron is crucial (all samples exhibited <1 at%) but the type of bonding, since the activity was most improved for the sample with the highest share in graphitic boron groups[12]. Thermochemical treatment of GF with phosphoric acid resulted in an enhanced electrode performance, revealing the formation of abundant pores in the range of 0.2 to 20 µm on the surface in addition

* Corresponding author.
E-mail address: hannes.radinger@kit.edu (H. Radinger).

https://doi.org/10.1016/j.electacta.2022.139971

to phosphorus-containing functional groups[13]. By nitrogen doping, the activity of GF for the $V^{V}O_2^{+}/V^{IV}O_{2+}$ redox reaction could be increased[14].

When the evaluation of heteroatom functionalization is the aim of a study, it is important to consider the effect of other activity-influencing properties. Often, the specific surface area is increased or additional edge sites are introduced, which greatly catalyze both vanadium half-cell reactions[10,17,18]. As a consequence, the proper influence of the integrated element cannot be addressed with certainty. Some researchers discussed the role of the heteroatom in general, since even bird dung was used to raise the electrocatalytic activity of graphene[19]. For doped materials, the increased activity is therefore secondary associated to the creation of abundant oxygen-containing functional groups[16,20]. These, however, do most probably not assist in the charge transfer process for the vanadium redox couple as our group has recently demonstrated[21].

It is therefore crucial to achieve a better understanding of the possible enhancement by heteroatom functionalization of graphitic surfaces. We first studied commercial boron (electron-withdrawing) and phosphorus (electron-donating) doped graphene by half-cell electrochemistry to elaborate on a heteroatom candidate. To establish correlations between the electrocatalytic and physicochemical characteristics, the bulk and surface properties of the material were studied in detail by X-ray diffraction, photoelectron and Raman spectroscopy. We also investigated the differences between the commercial and homemade modified graphene. Based on the thereby gained knowledge, GF was directly phosphorus-functionalized without changing the residual material properties which influence the activity. The modified GF was characterized by half-cell electrochemistry and full cell polarization curves. The underlying study thus provides evidence for the positive influence of heteroatom functionalization and paints a clear picture about the properties which are often changed as a side effect and can additionally have a enhancing or detrimental influence on the electrochemical activity.

2. Experimental

2.1. Sample preparation

To prepare graphene containing dispersions, 4 mg of pristine graphene (Dasheng graphene Co. Ltd., China), graphene treated at 3000 °C (G3000, Dasheng graphene Co. Ltd., China), boron and phosphorus-doped graphene (BG and PG-1, Sigma-Aldrich) powder were dispersed in 990 µL Milli-Q water (18.2 MΩ cm^{-1}) and 10 µL Nafion (5 wt%, Sigma-Aldrich) under ultrasonication for 90 min. 10 µL of the obtained homogeneous dispersion were drop coated with an Eppendorf pipette onto glassy carbon (GC) electrodes (ALS Co., Ltd.). Prior, the GC electrodes were polished with aluminum suspension (0.05 µm, MasterPrep, Buehler) on a polishing pad to mirror finish, and cleaned in acetone and Milli-Q under ultrasound. The coated electrodes were dried under ambient conditions for at least 1 h, rinsed with Milli-Q to remove residuals, and dried under nitrogen.

Phosphorus doped graphene (PG-2) was synthesized based on a method published elsewhere[22]. Briefly, 30 mg G3000 were dispersed in a solution containing 50 mL isopropanol and 150 mg triphenylphosphine (TPP, Sigma-Aldrich) for 2 h under ultrasound. The solvent was evaporated on a hot plate. The residual powder was homogenized in a mortar and heated in a corundum crucible with a ramp of 5 °C min^{-1} to 1000 °C for 90 min under argon atmosphere. After washing and drying, the final phosphorus doped powder was obtained.

Sheets of 4.6 mm thick pristine polyacrylonitrile-based graphite felt (GFD 4.6, SGL Carbon) were cut out and cleaned by sonication in acetone and Milli-Q for 10 min each, followed by drying at 80 °C overnight. To prepare graphene-modified electrodes, carboxymethyl cellulose (CMC, Sigma-Aldrich) was dissolved in Milli-Q water to a concentration of 1 mg mL^{-1}, and subsequently, 2 mg mL^{-1} graphene powder was added. The dispersion was ultrasonicated for 180 min to distribute the material homogeneously and durably[23]. The cleaned felts were dipped in the solution, thoroughly wetted by applying vacuum to the vessels, ultrasonicated for 20 min, reversed, and ultrasonicated again for the same time. Afterwards, the samples were transferred to a freeze-dryer (LyoQuest −85, Telstar), frozen overnight at −85 °C and then freeze-dried for 48 h. This procedure has proven to guarantee a homogeneous distribution of graphitic nanomaterials on GF[10]. The samples were subsequently heat-treated under argon atmosphere at 800 °C for 3 h to carbonize the binder.

The directly modified GF was fabricated by soaking the pristine felt with a TPP containing dimethyl sulfoxide (DMSO) solution (12.5, 25, and 50 mg mL^{-1}). The wet sample underwent the same freeze-drying process as described above and was subsequently heat-treated at 200 to 1000 °C under argon, either in an autoclave, in an open system, or in a closed graphite crucible with air holes.

The electrolyte for both half-cells was prepared by diluting sulfuric acid (98%, Emsure) in Milli-Q water to a concentration of 2 mol L^{-1}. The positive electrolyte was prepared by dissolving 0.1 M $VOSO_4 \times 5H_2O$ (Alfa Aesar) in 2 M H_2SO_4. To obtain the negative electrolyte, the positive half-cell electrolyte was reduced in a single cell assembly (MicroFlow cell, ElectroCell). It was added to both half-cell tanks, pumped through the single cell in a circuit, and charged at 1.6 V. The $V^{IV}O^{2+}$ is thus oxidized to $V^{V}O_2^{+}$ on one side and reduced to V^{III} on the other. At a termination current of 5 mA cm^{-2}, it was assumed that all the vanadium on the negative side was reduced to V^{III}.

2.2. Half-cell electrochemistry

A three-electrode glass cell was used to measure the drop-casted graphene electrodes. The sample served as the working, a graphite rod (redox.me) as the counter, and Ag/AgCl [3 M KCl, ALS Co. Ltd., ($E_{Ag/AgCl}$ = 0.210 V vs. RHE)] as the reference electrode. Before the electrochemical testing, the electrolyte was deaerated with argon. All electrochemical tests were performed using a Bio-Logic VSP potentiostat at room temperature, employing a scan rate of 10 mV s^{-1} in a potential range of −1 to 1.6 V vs. Ag/AgCl for cyclic voltammetry (CV) and linear sweep voltammetry (LSV).

For the investigation of GF, a custom-built three-electrode cell was used, and the graphite rod was exchanged for high area GF. GF pieces with a diameter of 7 mm were punched out of the sample and assembled in the electrochemical cell. CV was conducted with a slow scan rate of 1 mV s^{-1}. Electrochemical impedance spectroscopy (EIS) was recorded at an applied potential of −0.45 V vs. Ag/AgCl in the negative and 0.9 V vs. Ag/AgCl in the positive half-cell to assess the charge-transfer resistance (R_{CT}) of the respective vanadium redox reaction. The spectra were fitted with the RelaxIS 3 software (rhd instruments) using following equivalent circuit: an inductor and the electrolyte resistance in series, followed by two parallel resistance/constant phase elements, one for the glassy carbon/felt interface and one for the felt/electrolyte interface, and finally a constant phase element for diffusion (which was not always necessary). At the second interface, R_{CT} was evaluated. The electrical double layer capacitance (EDLC) was measured in a potential window of 0.15 to 0.25 V vs. Ag/AgCl. The potential was kept at 0.2 V vs. Ag/AgCl for 30 s before scanning the potential region with a given scan rate. Considering the anodic and cathodic current at 0.2 *vs.* Ag/AgCl, the slope of a current *vs.* scan rate plot reveals the capacitance C according to the equation $C = \frac{i \times t}{E}$, with i resembling the current, t the time, and E the potential.

2.3. Full cell electrochemistry

The characterization of the performance of GF under operational conditions was conducted by using an in-house designed single-cell VFB, assembled as zero-gap architecture. A graphite foil (GF-176, Graphite Materials GmbH) served as current collector. The electrodes (1×1 cm²) were fixed by a Teflon® (DuPont de Nemours Corp) spacer-layer, which was sandwiched between graphite foil and a separator membrane (Fumasep® FS-930, Fumatech BWT GmbH). A double-headed peristaltic pump (323Du, Watson-Marlow Pumps Group) ensured a continuous flow of the electrolyte (1.6 M V, $V^{III}/V^{IV} \approx 0.8/0.8$ M, 3 M H_2SO_4, 0.4 L per half-cell, GfE GmbH). The current collectors were connected to the potentiostat (Reference 3000, Gamry instruments) *via* gilded steel clamps (BU-60 G, Mueller Electric Europe LTD, UK).

The electrochemical protocol consisted of the three steps: (I) charging of the electrolyte, (II) equilibration of the electrode, and (III) the actual characterization *via* the polarization curve method. (I) To charge the electrolyte to a state of charge (SoC) $\gtrapprox$50%, it was galvanostatically charged at a current density of 68 mA cm^{-2} and a flow rate of 70 mL min^{-1} in an external cell. When the open circuit voltage reached 1.4 V, the electrolytes were directed *via* three-way valves to other liquid lines, which were connected to the actual test cell containing the electrode. (II) To equilibrate the electrode, the potentiostat generated short time alternating galvanostatic pulses of 1 s, whereby the step size was 1 mA cm^{-2}. When the cell-voltage reached ±200 mV of the open circuit voltage, one of ten equilibration cycle was finished. (III) The first galvanostatic discharge step at −10 mA cm^{-2} was generated for 30 s. Subsequently, steps with −20, −30, −40 mA cm^{-2}, *etc.*, (30 s each), resulted in a staircase-like electrical current *vs.* time profile. During these steps, the cell voltage was recorded. The discharge polarization curve was stopped at a cell voltage of 0 V. To show cell voltages at steady state conditions and to exclude the influence of capacitive voltages, the voltage over the last 10 s of each step was averaged. During the first polarization curve, the flow rate was 130 mL min^{-1}. Afterwards, an identical charging polarization curve was performed. Subsequently, the routine was repeated at flow rates of 100 and 70 mL min^{-1}. Current collectors, membranes and the electrolyte were exchanged for each sample.

2.4. Physicochemical characterization

Raman spectra were recorded with a LabRAM HR Evolution spectrometer (HORIBA Scientific), equipped with a HeNe laser (632.8 nm, E_{laser} = 1.9876 eV), further using a 600 grooves mm^{-1} grating and a 100× magnification objective. At least five spectra were averaged for each sample. All spectra were subtracted by a spline background, normalized to the highest signal and deconvoluted with absolute Lorentzian (D, G, D') and Gaussian-Lorentzian (D* and D'') peak shapes (Figure S1).

X-ray photoelectron spectroscopy (XPS) was performed using a K-alpha$^+$ spectrometer (Thermo Fisher Scientific) with monochromatic Al-K$_\alpha$ radiation ($E_{h\nu}$ = 1486.6 eV) at a spot size of ~400 µm. Survey spectra were recorded with a pass energy of 200 eV, detail spectra with 50 eV. The Thermo Avantage software was used for data acquisition and deconvolution, determining a Shirley background with the implemented smart background function. In the C 1 s region, the asymmetry of sp^2 hybridized graphitic carbon was evaluated with a tail mix of 80 to 90% and a tail exponent of 0.03 to 0.1. All other components were fitted using conventional Gaussian-Lorentzian peak profiles with FWHM values of up to 1.8 eV, restricting the position concerning the sp^2 signal and the relative FWHM (±0.1) to sp^3 hybridized carbon.

The X-ray diffraction patterns were measured with a STOE STADI P powder diffractometer using monochromatic Cu-Kα_1 radiation (λ = 1.54056 Å) in transmission geometry.

The electrical conductivity under compression was tested using a uniaxial compression device (zwickiLine, Zwick/Roell) with a 100 N load cell. The thickness of GF at no compression was calculated by the distance of the tools at 0.1 N. By knowing the thickness at a given force, the compression is derived. The test machine was coupled to a custom-built cell to measure the electrical conductivity. Gold-coated copper pins connected to a potentiostat (BioLogic SP-300) were attached to the load cell; YSZ insulating plates prevented short circuiting through the device. The voltage was measured at a current of 100 mA, and the area specific resistance calculated by $\rho_{el} = R \times A$, with R being the electrical resistance and A the felt contact area. To receive a standard deviation, three samples were tested for each modification.

3. Results and discussion

3.1. Graphene powder attached to GF

To investigate the influence of doped graphene on the electrochemical performance, the commercial powders (graphene: G, phosphorus-doped: PG-1, boron-doped: BG) were successfully attached to GF by a previously introduced method[10]. Scanning electron microscopy (SEM) images visualized the distribution of small particles at the intersection of fibers or on single fiber surfaces, and the absence of big aggregates in the pores (Figure S2). In the X-ray photoelectron P 2p spectrum of GF-PG (Figure S3), <1 at% phosphorus is identified, predominantly bound to three carbon and one oxygen atoms (C_3PO).

Cyclic voltammetry (CV) was used to study the values for the peak separation potential (ΔE_p) of the V^{III}/V^{II}, *i.e.*, the negative, and $V^{V}O_2^{+}/V^{IV}O^{2+}$ redox couple, *i.e.*, the positive half-cell reaction (**Fig. 1**). The activity of pristine GF (260 mV) in the negative half-cell (Fig. 1a) was improved by the attached graphene (160 mV). No major additional improvement was observed using the doped material. GF-PG-1 revealed a slightly lowered ΔE_p (150 mV) and higher peak currents. The $V^{V}O_2^{+}/V^{IV}O^{2}$ oxidation (Fig. 1b) was enhanced for GF-G, but the reduction was kinetically hindered, which results in the same ΔE_p as for GF (250 mV). Minor improvements were monitored for the doped material (230 and 220 mV).

The charge-transfer resistance (R_{CT}) of the respective redox reaction was studied using electrochemical impedance spectroscopy (EIS). In the negative half-cell (Fig. 1c), the R_{CT} of GF was 93.5 Ω cm_{geo}^{-2}, while GF-PG-1 showed a much lower value (34 Ω cm_{geo}^{-2}). For GF-BG (47 Ω cm_{geo}^{-2}) no improvement was found in comparison to the felt modified using undoped graphene (42 Ω cm_{geo}^{-2}). The R_{CT} was also reduced in the positive half-cell from 67.5 to 28.5 Ω cm_{geo}^{-2}, especially by the attached phosphorus-doped graphene (Fig. 1d). Even though the electrocatalytic activity of GF could be improved by attaching doped graphene, the possibilities of heteroatom doping must be studied in more detail to understand the important material properties for efficient electrode improvement.

3.2. Electrocatalytic activity of doped graphene powder

The electrocatalytic activity of the pure commercial material was studied. For referential purpose, a CV curve was recorded for a blank glassy carbon (GC) electrode and drop-casted graphene powder (**Fig. 2**a). We used two commercial graphene powders, of which one was heat-treated under inert gas at 3000 °C to heal defects and remove surface groups. In contrast to heat-treated G3000, pristine graphene showed a pre-located sharp redox peak below

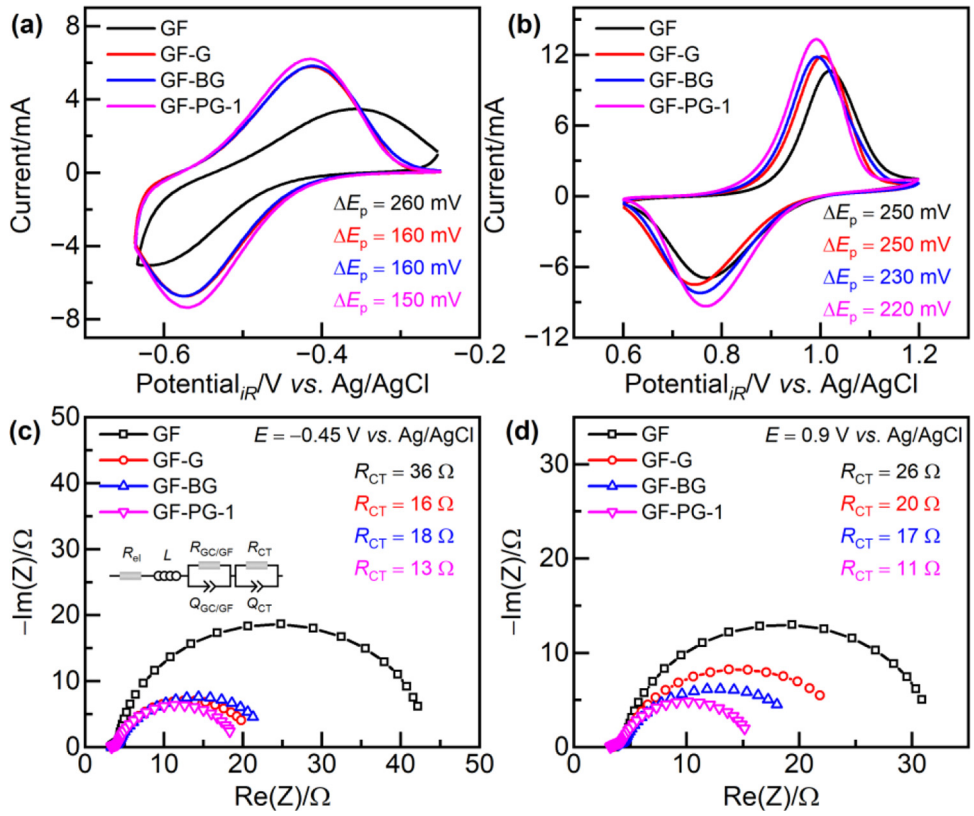

Fig. 1. Electrocatalytic activity of graphene-modified GF. **(a,b)** CV investigation of the **(a)** negative (V^{III}/V^{II}) and **(b)** positive ($V^{V}O_2^{+}/V^{IV}O^{2+}$) half-cell redox reactions with a scan rate of 1 mV s^{-1}. The respective peak potential separation (ΔE_p) is indicated. **(c,d)** EIS in the (c) negative and (d) positive half-cell at an applied potential to assess R_{CT}.

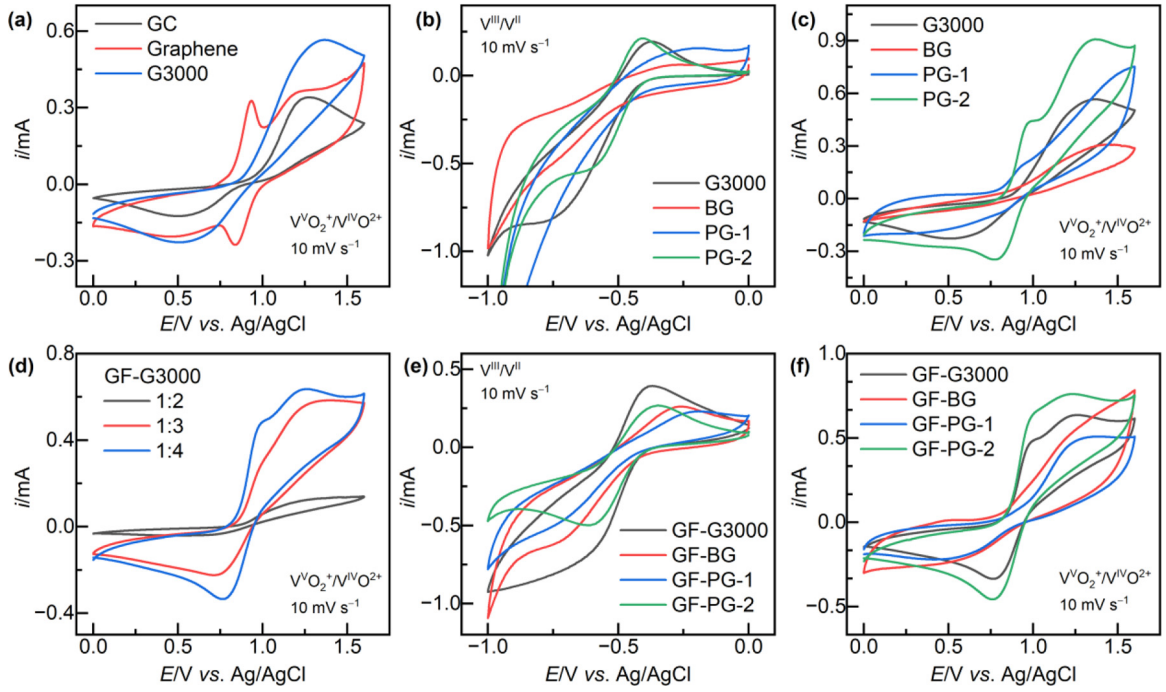

Fig. 2. CV investigation of drop-coated carbon-based material. **(a)** Blank GC and two different graphene powders. **(b,c)** Defect-free graphene (G3000) and doped graphene in the (b) negative and (c) positive half-cell. **(d)** A mixture of pulverized GF and G3000 at different mass ratios. **(e,f)** G3000 and doped graphene mixed with GF in a ratio of 1 to 4 in the (e) negative and (f) positive half-cell.

1 V *vs*. Ag/AgCl. The higher catalytic activity of graphene was associated with an increased degree of disorder, which resembled the presence of active defects such as edge sites. To demonstrate this, basal and edge plane exposed highly oriented pyrolytic graphite electrodes were investigated, revealing improved redox kinetics for the edges (Figure S4)[17,24]. We assume that the double peak structure is thus caused by a splitting of the redox signals when vanadium is reduced/oxidized either at basal planes or more active edges sites. The additional active defects of graphene were furthermore well-visible in the corresponding Raman spectra (Figure S5). The defect-poor G3000 was thus chosen as a reference for the doped material.

In both half-cell electrolytes (Fig. 2b,c), the boron-doped graphene provided a lower electrocatalytic activity than G3000, observed by a low current response and undefined peaks. Although PG-1 was rather inactive towards both half-cell reactions, a small $V^{V}O_2^{+}/V^{IV}O^{2+}$oxidation peak similar to defective graphene was visible. Due to these promising results, we synthesized phosphorus-doped graphene (PG-2) using a published method[25]. It showed improved redox kinetics and developed distinct peaks in both half-cells. However, rising currents toward the hydrogen and oxygen evolution reaction were detected. This was further examined in a vanadium-free sulfuric acid electrolyte (Figure S6), showing that PG-2 is active for these side reactions.

As a next step, we studied the activity of the doped material interacting with a graphite-based matrix, *i.e*., in contact with the felt, to converge the results observed for graphene-modified GF. Pristine GF was pulverized but could not be dispersed in a variety of solvents (H_2O, DMSO, IPA), even with the addition of a surfactant or binder. Therefore, it was mixed with G3000 in different ratios to force a homogeneous dispersion of aggregates by π–π stacking and drop casted on GC to study the catalytic activity (Fig. 2d). Adding four times the mass of G3000 to GF, a homogeneous dispersion was obtained, which was directly observed using CV by the formation of two distinct redox peaks. This ratio was thus chosen for the investigation of the doped material in both half-cell electrolytes (Fig. 2e,f). PG-2 showed well-defined redox peaks in the negative electrolyte, lower selectivity toward hydrogen evolution, and the highest currents in the positive electrolyte, whereas BG and PG-1 remained rather inactive.

3.3. Physicochemical characterization of doped graphene

To establish relationships between chemical and microstructural properties and the catalytic activity of the material, X-ray diffraction (XRD), Raman spectroscopy and X-ray photoelectron spectroscopy (XPS) were employed. By XRD, the degree of graphitization was analyzed (Fig. 3a). Graphite powder was used as a reference, showing Bragg reflections corresponding to the 002, 100, 101, 004, 110, and 112 planes located at 2θ = 26.5, 42.4, 44.7, 54.6, 77.5, and 83.6°, respectively[26]. These reflections were equally present for G3000 and PG-2. In contrast, the commercial PG-1 and especially BG revealed an amorphous appearance.

Structural differences were further studied by Raman spectroscopy (Fig. 3b). The main features of a graphite Raman spectrum constitute the G band at ∼1580 cm^{-1}, resembling the in-plane stretching of C=C bonds, and the D band at ∼1330 cm^{-1}, induced by disordering such as edge sites[27,28]. At higher wavenumbers, a second-order D band (2D) at 2655 cm^{-1}, characteristic for highly graphitic material, is visible[29]. The intensity ratio of the D and G band provides useful information such as the degree of disorder in the sample[30,31]. The heat-treated G3000 had a low $I(D)/I(G)$ ratio of 0.07, which was slightly increased to 0.13 due to the doping procedure for PG-2. In contrast, the commercial BG (1.89) and PG-1 (1.76) showed a high degree of disorder and a vanishing 2D signal, correlating to the amorphous XRD pattern.

The chemical composition was analyzed by XPS (Fig. 3c–g, S7). In the O 1 s detail spectra of G3000 (Fig. 3c), three different carbon–oxygen components were identified: carbonyls (O=C) at ∼531.1 eV, hydroxyls (O=C) at ∼532.1 eV, and carboxylic groups (O=C–O) at ∼533.1 eV[32–34]. An additional oxygen component was present for BG and PG-1 at ∼530.9 and 530.7 eV, arising from oxygen bound to boron or phosphorus, respectively. Six different contributions in the C 1 s region (Fig. 3d) were visible for all samples: sp^2 hybridized carbon at ∼284.4 eV, sp^3 related carbon at ∼285.2 eV, and carbonaceous components at ∼286.7 to 289.6 eV[16,35]. For BG, boron (∼3.1 at%) was equally bound to three carbon atoms in the basal plane (190.9 eV), and at the edge site to two carbon and one oxygen atom (192.4 eV)[36,37]. PG-1 reveals phosphorus (∼2.4 at%) majorly coordinated to one or two carbon atoms (133.4 eV), and the lesser amount covalently substituted in the graphite lattice (132.1 eV). Additionally, elemental phosphorus was present (129.6 eV). In contrast, PG-2 (Figure S8) had a lower doping concentration of <1 at%, further exhibiting a lower share in edge site located and no elemental phosphorus.

Close to the Fermi level (E_F), more information about the electronic structure of the material was assessed (Fig. 3g). The domains below E_F are occupied by C 2p (2 to 12 eV), C 2 s (to 22 eV), and O 2 s (above 22 eV) valence electrons[38–40]. A sharp signal for BG at ∼16 eV corresponded to the B 2 s core level. All samples showed a non-zero state between 0 and 3 eV due to 2p–π electrons in the basal plane[41]. The steep onset of electron density for G3000 (∼3 eV) shifted to lower values for BG (2.6) and PG-1 (2.1). This suggests that a higher electron density exists close to E_F and could in theory more easily participate in charge transfer reactions. However, especially for PG-1, this uplift was not reflected in the catalytic activity.

In contrast to the electron enrichment in the valence band (Fig. 3g) and the high number of defects for the doped graphene characterized by XPS and Raman spectroscopy, several properties were observed which influence the activity negatively. We recently demonstrated that surface oxygen inhibits the electron transfer, which could explain the poorer performance of BG (∼10 at%) and PG-1 (∼11 at%) sample compared to PG-2 (<1 at%)[10,21]. In an elemental analysis (Table S1), an even lower carbon content for the commercial powders (76 to 78%) was revealed. The high degree of bulk oxygen is suspected to impede the electrical conductivity. The amorphous XRD pattern and a broadened sp^2 carbon feature (from 0.8 to 1 eV) in the photoelectron spectra demonstrated low long-range order and decreased graphitic character at the surface, both detrimental for the catalytic activity[42,43]. Considering the higher dopant concentration of PG-1 (∼2.4 at%) compared to PG-2 (<1 at%), the number of foreign atoms in the structure might not define the catalytic activity. Instead, it could be more important how the phosphorus is embedded in the lattice. In our case, a low number of mainly graphitic coordinated phosphorus (C_3PO) was responsible for a remarkable change of the electrochemical performance. In summary, for a material which maintains low degree of oxygenation and high long-range order, phosphorus-doping could be a suitable strategy to improve the electrocatalytic activity.

3.4. Directly phosphorus-doped GF

After the previous investigation, phosphorus-doped material stood out as a promising way to improve the electrocatalytic activity, suggesting that electron-donating species could be beneficial. The discrepancy between our and previous published results may be resolved considering that most modification techniques go along with significant changes not only to the surface chemistry, but also alter morphology and the nature and density of other graphitic defects. As has been shown by our previous works, these changes alone may explain a significant part of the observed cat-

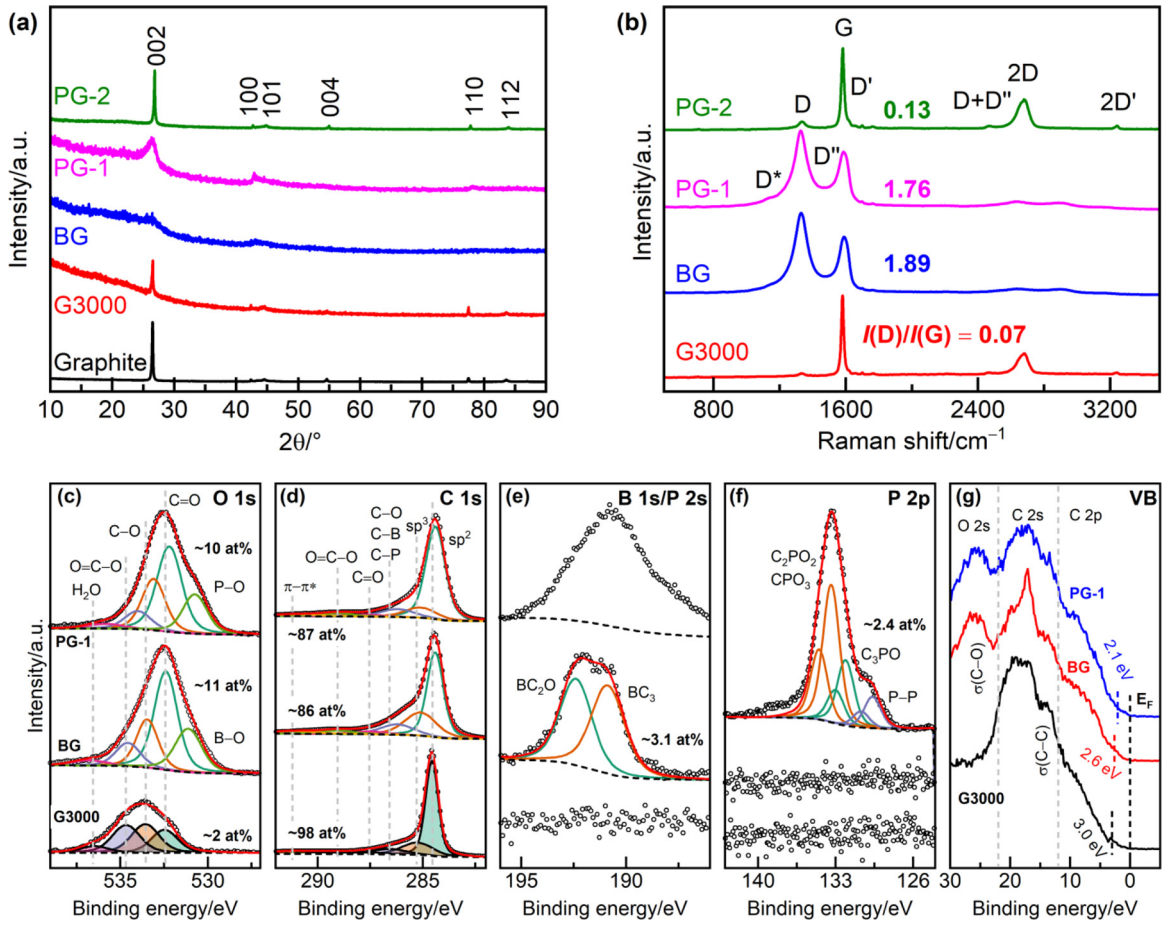

Fig. 3. Physicochemical characterization of pristine and doped graphene. **(a)** XRD pattern with graphite powder as reference. **(b)** Raman spectra with the assigned vibrational features and the evaluated D to G ratio. **(c–f)** Deconvoluted XPS detail regions of the (c) O 1 s, (d) C 1 s, (e) B 1 s/P 2 s, and (f) P 2p signals. The respective concentration of each element is indicated, and the single species are assigned regarding their binding energy position. **(g)** The valence band (VB) region close to the Fermi level (E_F).

alytic improvement, either by increasing the active surface area or by improving the kinetics of the charge transfer. We therefore point out that it is essential to prevent changes in morphology and to monitor the density of graphitic defects when the effect of heteroatom functionalization is evaluated.

To study the effect of phosphorus surface functionalization for GF, a slightly modified method used for PG-2 was employed. To exclude any influence on other felt properties of the obtained GF-P, various analytical tools were used. By SEM, we ruled out that our treatment damaged the material visibly (Figure S9). In the XRD pattern (Fig. 4a), four out of six graphene reflections were present for both pristine GF and GF-P that did not differ concerning their positions, relative intensities, or FWHM values, proving that the modification had no effect on the internal structure.

The change of disorder was monitored by Raman spectroscopy (Fig. 4b). The D to G ratio of GF slightly increased from 1.95 to 2.05 due to the modification. Additional defects were also reflected in the relatively less intense 2D band. By XPS, the level of oxygenation was studied (Fig. 4c), since it was proposed that oxygen-rich phosphate groups can enhance the activity of GF, which we wanted to exclude as a possible influence[20]. The low oxygen content of the pristine felt (~7 at%) was maintained by our treatment. The phosphorus concentration was estimated to <1 at% by the analysis of the P 2p region (Fig. 4d). In contrast to other publications that deal with phosphorus functionalization of GF, herein it was not bound to carbon by an oxygen bridge as a functional group but directly substituted for a carbon atom in the graphite lattice, either in the basal plane (C_3PO) or at the edges (C_2PO_2/CPO_3)[13,20]. Due to the low increase in disorder and the absence of pores in the SEM images, we conclude that the changes in the electrochemical performance of GF-P can be associated mainly with the substitution. Similar to the doped graphene powders, it was seen in the valence band region that the treatment increased the electron density close to E_F by ~0.7 eV (Fig. 4e). Furthermore, a shift of the σ(C–O) signals toward the C 2p region was determined which corresponds to the presence of majorly hydroxyl and carboxylic groups over carbonyl and ether groups and agrees well with the observations in the O1s spectrum (Fig. 4c)[38].

The electrochemical half-cell performance of GF-P was studied in comparison to pristine GF and a felt treated analogous to GF-P, but in the absence of a phosphorus source (GF-1000). This was conducted since the performance of GF is already improved by a surface cleaning at high temperatures under argon atmosphere[21]. This could be seen by an improved ΔE_p for GF-1000 from 260 (GF) to 140 mV in the negative half-cell (**Fig. 5**a). However, the ΔE_p was further decreased to 80 mV for GF-P. Similarly, in the positive half-cell GF-P showed a lower ΔE_p (90 mV) than the less active GF (280 mV) and the thermally treated GF-1000 (140 mV) (Fig. 5b). The electrical double layer capacitance (EDLC) was studied to qualitatively compare the electrochemically active surface area[44]. The low EDLC of GF (~1.2 mF) was increased by a factor of ~5 due to the phosphorus-functionalization. The EDLC is mainly related to the graphitic disorder, as the basal plane has low values, followed by edge sites and carbon vacancies or point defects, as it is the case for GF-P[45]. A further investigation of the electrochemical impedance confirmed the success of the modification (Fig. 5d,e

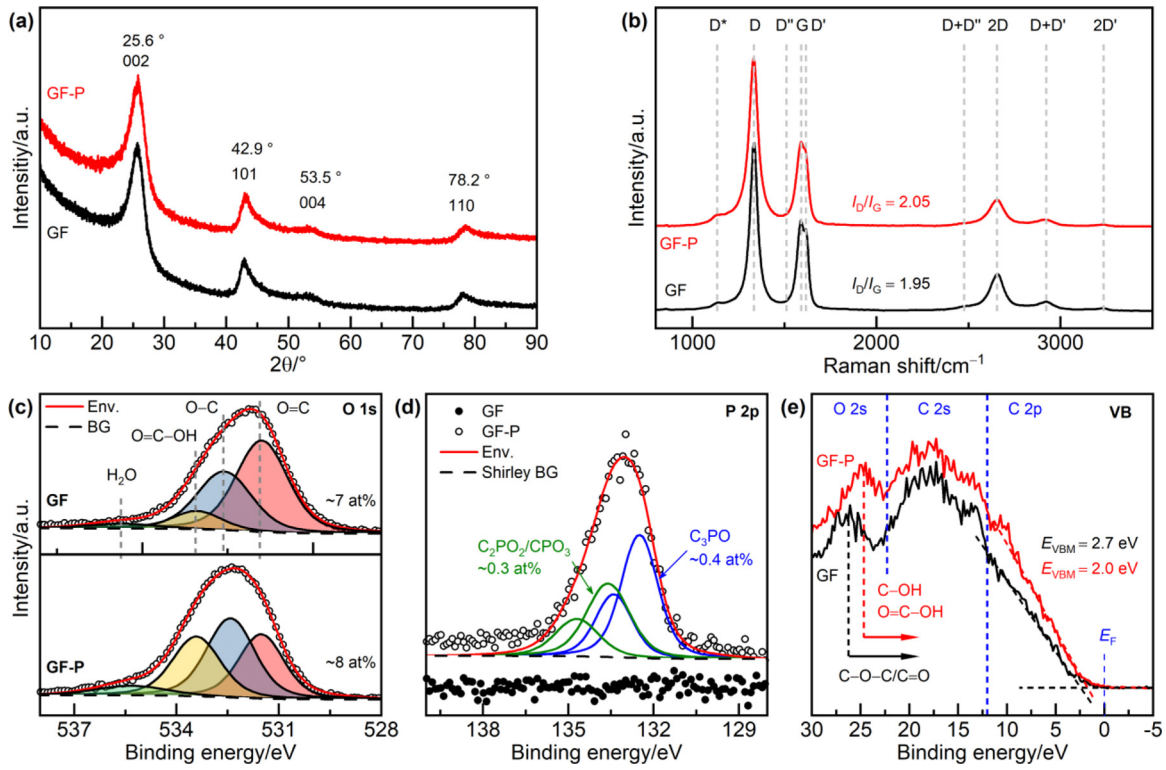

Fig. 4. Physicochemical characterization of GF and GF-P. The microstructural properties were analyzed by **(a)** XRD and **(b)** Raman spectroscopy. **(c–e)** XPS investigation of the (c) O 1 s and (d) P 2p detail regions, and the (e) valence band region.

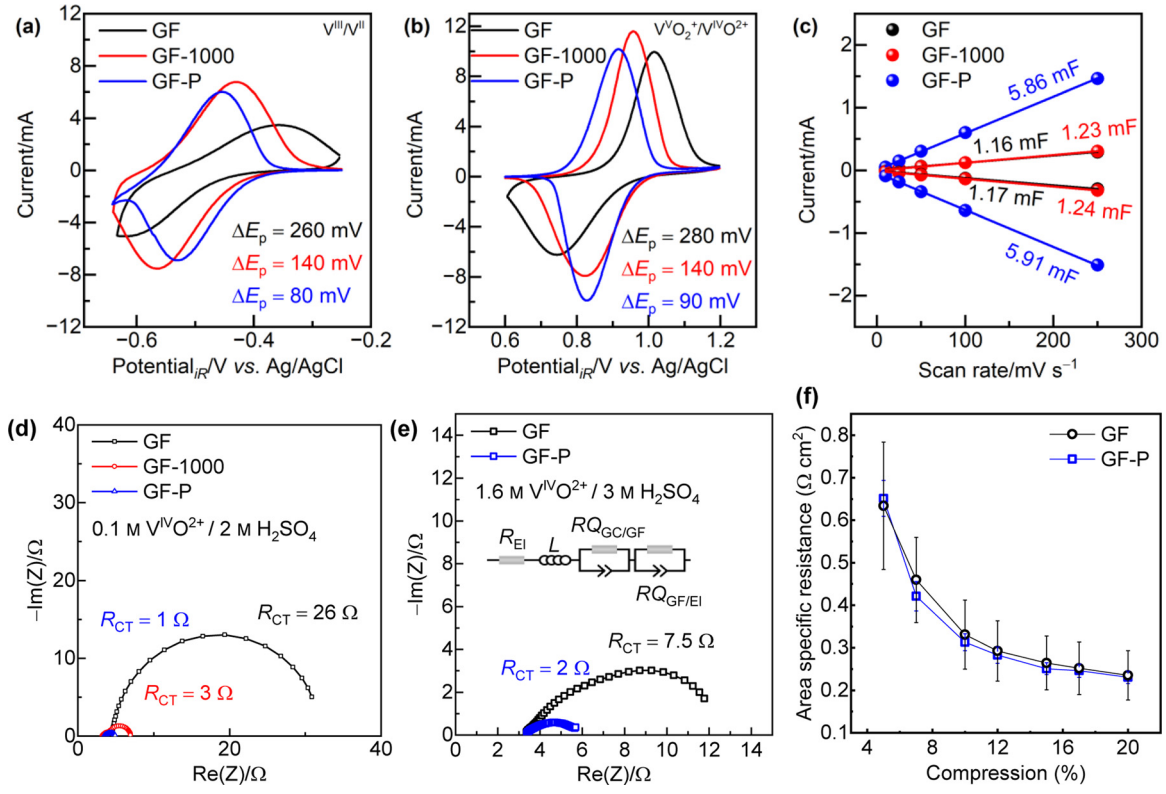

Fig. 5. Electrochemical half-cell performance and electrical conductivity of pristine and modified GF. CV was performed in the **(a)** negative and **(b)** positive half-cell. The peak potential separation ΔE_p is indicated. **(c)** EDLC assessed by CV in a non-faradaic potential window. The anodic and cathodic current responses are evaluated separately. **(d,e)** EIS at an applied potential of 0.9 V *vs.* Ag/AgCl in (d) half-cell and (e) full cell battery electrolyte. **(f)** Electrical conductivity under compression.

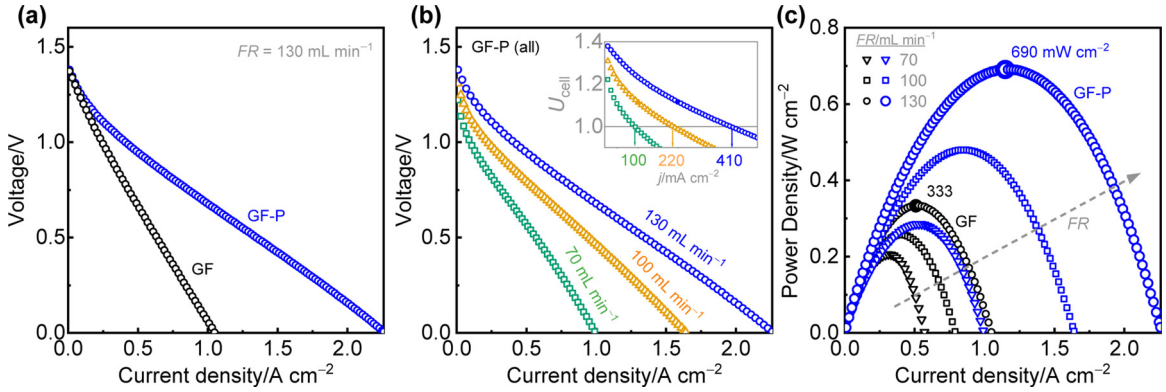

Fig. 6. Electrochemical full cell performance of GF and GF-P. **(a,b)** Polarization curves **(a)** at a flow rate (FR) of 130 mL min^{-1} and **(b)** at different flow rates. **(c)** Power curve at different FR.

and Figure S10) by lowered R_{CT} values in the negative half-cell from 101 (GF) over 49 (GF-1000) to 5 Ω cm_{geo}^{-2} (GF-P), and for the $V^{V}O_2^{+}/V^{IV}O^{2+}$ redox reaction from 67.5 to 2.5 Ω cm_{geo}^{-2}. Additionally, EIS measurements were repeated using the electrolyte composition of the below conducted full cell experiments. Whereas the R_{CT} value of GF-P remains unchanged at ~5 Ω cm_{geo}^{-2}, the slow reaction kinetics of pristine GF become less relevant, exposing a much lower R_{CT} of 19.5 Ω cm_{geo}^{-2} at higher vanadium and sulfuric acid concentrations. To study in more detail whether reduced R_{CT} values are a consequence of higher electrical conductivity, the area specific resistance under compression was evaluated (Fig. 5f). It is seen that there is no significant difference between GF and GF-P, marking faster reaction kinetics to be responsible for the enhanced electrocatalytic activity.

Several parameters, such as the heating temperature (Figure S11), the concentration of the precursor solution, and the reaction environment (Figure S12) were altered to find the optimum parameters for the synthesis of GF-P. The herein presented highly active GF-P exhibited a low heteroatom concentration of <1 at% using 25 mg mL^{-1} TPP, and required a heating temperature of 1000 °C in a closed reaction environment. The activity could not be further improved by increasing the molarity of the precursor solution.

To investigate the electrochemical performance of GF-P under nearly realistic operation conditions (*i.e.*, forced convection of the electrolyte through the electrodes), VFB test cells were equipped with the samples and the polarization curve method was conducted at SoC ≳50%. Thus it can be quantitatively and qualitatively distinguished between different types of voltage losses of kinetic activation, ohmic and mass-transport overpotentials[46]. The polarization curves of GF and GF-P at a flow rate of 130 mL min^{-1} are displayed in **Fig. 6**a. The progression of the *U vs. i* curves of GF-P and GF at low current densities shows the polarization losses due to the kinetic activation of the electrodes. While GF reaches a cell voltage of 1.0 V at already 240 mA cm², a current density of 410 mA cm² is required for GF-P. While GF-P clearly transits into a linear Ohmic loss region at about 1.2 V, this behavior is not very pronounced for GF. The phosphorus-functionalized felt further shows improved reaction kinetics in that region by a lower slope compared to pristine GF. A precise observation of the progressions of the *U vs. i* curves of GF-P especially reveals a decent exponential-like decrease at high current densities above 1.5 A cm², which is an indicator for mass transport overpotentials. For GF, a progression from a linear to an exponential-like region cannot be observed with certainty. This shows that the cell voltage was lowered by kinetic activation and by mass-transport overpotentials, which likely resulted from the slow kinetics of the V^{II} oxidation in comparison to the fast $V^{V}O_2^{+}$ reduction, especially pronounced for the active GF-P[47]. A cell voltage of 0.0 V was reached at current densities of 1.05 and 2.30 A cm², respectively, demonstrating the ability of GF-P to tolerate higher limiting currents. Despite of high educt availability (high in theory due to a high flow rate and high vanadium concentration), the lowering of the flow rate caused a 'forking' of the polarization curves even at very low current densities (Fig. 6b). The current density which is necessary to reach a potential of 1.0 V is dependent on the flow rate, increasing from 100 over 220 to 410 for flow rates of 70, 100, and 130 mL min^{-1}, respectively. In summary, we conclude that under realistic operational conditions, the superior GF-P electrode material scores by lower polarization losses, faster redox kinetics, and an improved availability/removal of educt/product, respectively, during the VFB discharge reaction. This is further expressed by the high peak power density in Fig. 6c of GF-P (690 mW cm^{-2}), which is more than twice as for GF (333 mW cm^{-2}).

4. Conclusions

In this work, the influence of phosphorus heteroatom functionalization on the electrochemical performance of graphene and GF was investigated. By using commercial in comparison to synthesized phosphorus-doped graphene, the important physicochemical properties of an active electrocatalyst for the vanadium redox reactions were assessed. A high degree of graphitization and low number of surface and bulk oxygen groups were considered necessary to profit from phosphorus as additional active site. The amorphous appearance and high surface as well as bulk oxygen content of the commercial powders were detrimental to the activity. Consequently, the rationally synthesized phosphorus-doped graphene showed a high electrocatalytic activity. We transferred our knowledge to realistic battery electrodes and successfully functionalized GF. The bulk and surface properties of GF were nearly unchanged, which demonstrates that changes in the electrochemical performance result from the heteroatom modification only. Subsequently, a high electrocatalytic activity was characterized for both half-cell reactions. Full cell polarization curves demonstrated reduced kinetic and ohmic losses, higher limiting currents and twice the power density of phosphorus-functionalized compared to pristine GF. Retaining important graphite properties such as a highly ordered sp^2 carbon content, low concentration of surface functional groups, and incorporation of phosphorus directly into the graphite lattice matters more than the sheer concentration of the heteroatom. This study showcases the importance of a holistic view on the surface modification of GF since one changing property cannot be made responsible for changes in the electrochem-

ical activity, when the other material characteristics are not observed equally.

Credit author statement

Hannes Radinger: Conceptualization, Methodology, Investigation, Writing - original draft
Mark Hartmann: Investigation, Writing - original draft
Marius Ast: Investigation
Jessica Pfisterer: Investigation
Michael Bron: Resources, Writing - review & editing
Helmut Ehrenberg: Resources
Frieder Scheiba: Resources, Writing - review & editing

Declaration of Competing Interest

The authors declare that they have no known competing financial interests or personal relationships that could have appeared to influence the work reported in this paper.

Acknowledgments

The financial support of the Federal Ministry of Education and Research (BMBF) within the project Flow3DKat (03EK3053C) is acknowledged. This work contributes to the research performed at CELEST (Center for Electrochemical Energy Storage Ulm-Karlsruhe). The authors thank Lihua Zhu for providing graphene powders. H.R. thanks Mattes Renner for sample preparation.

Supplementary materials

Supplementary material associated with this article can be found, in the online version, at doi:10.1016/j.electacta.2022.139971.

References

[1] A.M. Pezeshki, J.T. Clement, G.M. Veith, T.A. Zawodzinski, M.M. Mench, High performance electrodes in vanadium redox flow batteries through oxygen-enriched thermal activation, J. Power Sources 294 (2015) 333–338, doi:10.1016/j.jpowsour.2015.05.118.
[2] Z. He, Y. Jiang, W. Meng, F. Jiang, H. Zhou, Y. Li, J. Zhu, L. Wang, L. Dai, HF/H2O2 treated graphite felt as the positive electrode for vanadium redox flow battery, Appl. Surf. Sci. 423 (2017) 111–118, doi:10.1016/j.apsusc.2017.06.154.
[3] M.A. Miller, A. Bourke, N. Quill, J.S. Wainright, R.P. Lynch, D.N. Buckley, R.F. Savinell, Kinetic study of electrochemical treatment of carbon fiber microelectrodes leading to in situ enhancement of vanadium flow battery efficiency, J. Electrochem. Soc. 163 (2016) A2095–A2102, doi:10.1149/2.1091609jes.
[4] H. Radinger, 2021: a surface odyssey. The role of oxygen functional groups on activated carbon-based electrodes in vanadium flow batteries, Chem. Phys. Chem.. https://doi.org/10.1002/cphc.202100623.
[5] W. Li, Z. Zhang, Y. Tang, H. Bian, T.-W. Ng, W. Zhang, C.-S. Lee, Graphene-nanowall-decorated carbon felt with excellent electrochemical activity toward VO2+/VO2+ couple for all vanadium redox flow battery, Adv. Sci. 3 (2016) 1500276, doi:10.1002/advs.201500276.
[6] Y.-C. Chang, Y.-C. Shih, J.-Y. Chen, G.-Y. Lin, N.-Y. Hsu, Y.-S. Chou, C.-H. Wang, High efficiency of bamboo-like carbon nanotubes on functionalized graphite felt as electrode in vanadium redox flow battery, RSC Adv. 6 (2016) 102068–102075, doi:10.1039/C6RA22035E.
[7] B. Li, M. Gu, Z. Nie, Y. Shao, Q. Luo, X. Wei, X. Li, J. Xiao, C. Wang, V. Sprenkle, W. Wang, Bismuth nanoparticle decorating graphite felt as a high-performance electrode for an all-vanadium redox flow battery, Nano Lett. 13 (2013) 1330–1335, doi:10.1021/nl400223v.
[8] P.C. Ghimire, R. Schweiss, G.G. Scherer, N. Wai, T.M. Lim, A. Bhattarai, T.D. Nguyen, Q. Yan, Titanium carbide-decorated graphite felt as high performance negative electrode in vanadium redox flow batteries, J. Mater. Chem. A 6 (2018) 6625–6632, doi:10.1039/c8ta00464a.
[9] K. Amini, J. Gostick, M.D. Pritzker, Metal and metal oxide electrocatalysts for redox flow batteries, Adv. Funct. Mater. 30 (2020) 1910564, doi:10.1002/adfm.201910564.
[10] H. Radinger, J. Pfisterer, F. Scheiba, H. Ehrenberg, Influence and electrochemical stability of oxygen groups and edge sites in vanadium redox reactions, Chem. Electro. Chem. 7 (2020) 4745–4754, doi:10.1002/celc.202001387.
[11] A. Xu, L. Shi, L. Zeng, T.S. Zhao, First-principle investigations of nitrogen-, boron-, phosphorus-doped graphite electrodes for vanadium redox flow batteries, Electrochim. Acta 300 (2019) 389–395, doi:10.1016/j.electacta.2019.01.109.
[12] H.R. Jiang, W. Shyy, L. Zeng, R.H. Zhang, T.S. Zhao, Highly efficient and ultra-stable boron-doped graphite felt electrodes for vanadium redox flow batteries, J. Mater. Chem. A 6 (2018) 13244–13253, doi:10.1039/c8ta03388a.
[13] R. Wang, Y. Li, Y. Wang, Z. Fang, Phosphorus-doped graphite felt allowing stabilized electrochemical interface and hierarchical pore structure for redox flow battery, Appl. Energy 261 (2020) 114369, doi:10.1016/j.apenergy.2019.114369.
[14] S. Park, H. Kim, Fabrication of nitrogen-doped graphite felts as positive electrodes using polypyrrole as a coating agent in vanadium redox flow batteries, J. Mater. Chem. A 3 (2015) 12276–12283, doi:10.1039/C5TA02674A.
[15] V. Pasala, J.N. Ramavath, C. He, V.K. Ramani, K. Ramanujam, N- and P-co-doped graphite felt electrode for improving positive electrode chemistry of the vanadium redox flow battery, Chem. Sel. 3 (2018) 8678–8687, doi:10.1002/slct.201801446.
[16] M. Park, J. Ryu, Y. Kim, J. Cho, Corn protein-derived nitrogen-doped carbon materials with oxygen-rich functional groups: a highly efficient electrocatalyst for all-vanadium redox flow batteries, Energy Environ. Sci. 7 (2014) 3727–3735, doi:10.1039/C4EE02123A.
[17] N. Pour, D.G. Kwabi, T. Carney, R.M. Darling, M.L. Perry, Y. Shao-Horn, Influence of edge- and basal-plane sites on the vanadium redox kinetics for flow batteries, J. Phys. Chem. C 119 (2015) 5311–5318, doi:10.1021/jp5116806.
[18] D. Dixon, D.J. Babu, A. Bhaskar, H.-.M. Bruns, J.J. Schneider, F. Scheiba, H. Ehrenberg, Tuning the performance of vanadium redox flow batteries by modifying the structural defects of the carbon felt electrode, Beilstein J. Nanotechnol. 10 (2019) 1698–1706, doi:10.3762/bjnano.10.165.
[19] L. Wang, Z. Sofer, M. Pumera, Will any crap we put into graphene increase its electrocatalytic effect? ACS Nano 14 (2020) 21–25, doi:10.1021/acsnano.9b00184?ref=pdf.
[20] K.J. Kim, H.S. Lee, J. Kim, M.-S. Park, J.H. Kim, Y.-J. Kim, M. Skyllas-Kazacos, Superior electrocatalytic activity of a robust carbon-felt electrode with oxygen-rich phosphate groups for all-vanadium redox flow batteries, Chem. Sus. Chem. 9 (2016) 1329–1338, doi:10.1002/cssc.201600106.
[21] H. Radinger, A. Ghamlouche, H. Ehrenberg, F. Scheiba, Origin of the catalytic activity at graphite electrodes in vanadium flow batteries, J. Mater. Chem. A 9 (2021) 18280–18293, doi:10.1039/D1TA04316A.
[22] A.R. MacIntosh, G. Jiang, P. Zamani, Z. Song, A. Riese, K.J. Harris, X. Fu, Z. Chen, X. Sun, G.R. Goward, Phosphorus and nitrogen centers in doped graphene and carbon nanotubes analyzed through solid-state NMR, J. Phys. Chem. C 122 (2018) 6593–6601, doi:10.1021/ACS.JPCC.7B11671.
[23] L. Jia, Y. Chen, S. Lei, S. Mo, Z. Liu, X. Shao, Effect of magnetic field and surfactant on dispersion of graphene/water nanofluid during solidification, Energy Procedia 61 (2014) 1348–1351, doi:10.1016/j.egypro.2014.12.124.
[24] S.M. Taylor, A. Pătru, D. Perego, E. Fabbri, T.J. Schmidt, Influence of carbon material properties on activity and stability of the negative electrode in vanadium redox flow batteries: a model electrode study, ACS Appl. Energy Mater. 1 (2018) 1166–1174, doi:10.1021/acsaem.7b00273.
[25] F. Niu, L.-M. Tao, Y.-C. Deng, Q.-H. Wang, W.-G. Song, Phosphorus doped graphene nanosheets for room temperature NH3 sensing, New J. Chem. 38 (2014) 2269, doi:10.1039/c4nj00162a.
[26] Z.Q. Li, C.J. Lu, Z.P. Xia, Y. Zhou, Z. Luo, X-ray diffraction patterns of graphite and turbostratic carbon, Carbon N Y 45 (2007) 1686–1695, doi:10.1016/j.carbon.2007.03.038.
[27] F. Tuinstra, J.L. Koenig, Raman spectrum of graphite, J. Chem. Phys. 53 (1970) 1126–1130, doi:10.1063/1.1674108.
[28] R.P. Vidano, D.B. Fischbach, L.J. Willis, T.M. Loehr, Observation of Raman band shifting with excitation wavelength for carbons and graphites, Solid State Commun. 39 (1981) 341–344, doi:10.1016/0038-1098(81)90686-4.
[29] M.S. Dresselhaus, A. Jorio, R. Saito, Characterizing graphene, graphite, and carbon nanotubes by raman spectroscopy, Annu. Rev. Condens. Matter Phys. 1 (2010) 89–108, doi:10.1146/annurev-conmatphys-070909-103919.
[30] M.A. Pimenta, G. Dresselhaus, M.S. Dresselhaus, L.G. Cançado, A. Jorio, R. Saito, Studying disorder in graphite-based systems by Raman spectroscopy, Phys. Chem. Chem. Phys. 9 (2007) 1276–1291, doi:10.1039/b613962k.
[31] M.S. Dresselhaus, A. Jorio, A.G. Souza Filho, R. Saito, Defect characterization in graphene and carbon nanotubes using Raman spectroscopy, Philos. Trans. R. Soc. London, Ser. A 368 (2010) 5355–5377, doi:10.1098/rsta.2010.0213.
[32] C.-H. Chuang, S.C. Ray, D. Mazumder, S. Sharma, A. Ganguly, P. Papakonstantinou, J.-W. Chiou, H.-M. Tsai, H.-W. Shiu, C.-H. Chen, H.-J. Lin, J. Guo, W.-F. Pong, Chemical modification of graphene oxide by nitrogenation: an X-ray absorption and emission spectroscopy study, Sci. Rep. 7 (2017) 42235, doi:10.1038/srep42235.
[33] G. Wang, C. Feng, Electrochemical polymerization of hydroquinone on graphite felt as a pseudocapacitive material for application in a microbial fuel cell, Polymers (Basel) 9 (2017), doi:10.3390/polym9060220.
[34] L. Tang, X. Li, R. Ji, K.S. Teng, G. Tai, J. Ye, C. Wei, S.P. Lau, Bottom-up synthesis of large-scale graphene oxide nanosheets, J. Mater. Chem. 22 (2012) 5676, doi:10.1039/c2jm15944a.
[35] T.H. Lim, S.Y. Yeo, Investigation of the degradation of pitch-based carbon fibers properties upon insufficient or excess thermal treatment, Sci. Rep. 7 (2017) 4733, doi:10.1038/s41598-017-05192-5.
[36] W. Cheng, X. Liu, N. Li, J. Han, S. Li, S. Yu, Boron-doped graphene as a metal-free catalyst for gas-phase oxidation of benzyl alcohol to benzaldehyde, RSC Adv 8 (2018) 11222–11229, doi:10.1039/c8ra00290h.
[37] N. Sreekanth, M.A. Nazrulla, T.V. Vineesh, K. Sailaja, K.L. Phani, Metal-free boron-doped graphene for selective electroreduction of carbon dioxide to formic acid/formate, Chem. Commun. 51 (2015) 16061–16064, doi:10.1039/C5CC06051F.

[38] A. Ganguly, S. Sharma, P. Papakonstantinou, J. Hamilton, Probing the thermal deoxygenation of graphene oxide using high-resolution in situ X-ray-based spectroscopies, J. Phys. Chem. C 115 (2011) 17009–17019, doi:10.1021/jp203741y.
[39] M. Jin, T.H. Kim, S.C. Lim, D.L. Duong, H.J. Shin, Y.W. Jo, H.K. Jeong, J. Chang, S. Xie, Y.H. Lee, Facile physical route to highly crystalline graphene, Adv. Funct. Mater. 21 (2011) 3496–3501, doi:10.1002/adfm.201101037.
[40] F.R. McFeely, S.P. Kowalczyk, L. Ley, R.G. Cavell, R.A. Pollak, D.A. Shirley, X-ray photoemission studies of diamond, graphite, and glassy carbon valence bands, Phys. Rev. B 9 (1974) 5268–5278, doi:10.1103/PhysRevB.9.5268.
[41] M.K. Rabchinskii, S.A. Ryzhkov, D.A. Kirilenko, N.V. Ulin, M.V. Baidakova, V.V. Shnitov, S.I. Pavlov, R.G. Chumakov, D.Y. Stolyarova, N.A. Besedina, A.V. Shvidchenko, D.V. Potorochin, F. Roth, D.A. Smirnov, M.V. Gudkov, M. Brzhezinskaya, O.I. Lebedev, V.P. Melnikov, P.N. Brunkov, From graphene oxide towards aminated graphene: facile synthesis, its structure and electronic properties, Sci. Rep. 10 (2020) 6902, doi:10.1038/s41598-020-63935-3.
[42] J. Melke, P. Jakes, J. Langner, L. Riekehr, U. Kunz, Z. Zhao-Karger, A. Nefedov, H. Sezen, C. Wöll, H. Ehrenberg, C. Roth, Carbon materials for the positive electrode in all-vanadium redox flow batteries, Carbon N Y 78 (2014) 220–230, doi:10.1016/j.carbon.2014.06.075.
[43] J. Langner, M. Bruns, D. Dixon, A. Nefedov, C. Wöll, F. Scheiba, H. Ehrenberg, C. Roth, J. Melke, Surface properties and graphitization of polyacrylonitrile based fiber electrodes affecting the negative half-cell reaction in vanadium redox flow batteries, J. Power Sources 321 (2016) 210–218, doi:10.1016/j.jpowsour.2016.04.128.
[44] R.E. Smith, T.J. Davies, N.d.B. Baynes, R.J. Nichols, The electrochemical characterisation of graphite felts, J. Electroanal. Chem. 747 (2015) 29–38, doi:10.1016/j.jelechem.2015.03.029.
[45] Z. Li, H. Peng, R. Liu, Y. Mo, B. Cao, W. Lai, X. Li, L. Pan, Y. Chen, Quantitative assessment of basal-, edge- and defect-surfaces of carbonaceous materials and their influence on electric double-layer capacitance, J. Power Sources 457 (2020) 228022, doi:10.1016/j.jpowsour.2020.228022.
[46] D.S. Aaron, Q. Liu, Z. Tang, G.M. Grim, A.B. Papandrew, A. Turhan, T.A. Zawodzinski, M.M. Mench, Dramatic performance gains in vanadium redox flow batteries through modified cell architecture, J. Power Sources 206 (2012) 450–453, doi:10.1016/j.jpowsour.2011.12.026.
[47] M.-.A. Goulet, M. Eikerling, E. Kjeang, Direct measurement of electrochemical reaction kinetics in flow-through porous electrodes, Electrochem. Commun. 57 (2015) 14–17, doi:10.1016/j.elecom.2015.04.019.